Available online at www.sciencedirect.com
SCIENCE DIRECT®
Journal of Nuclear Materials 326 (2004) 175–184
journal of nuclear materials
www.elsevier.com/locate/jnucmat

A model for the influence of microstructure, precipitate pinning and fission gas behavior on irradiation-induced recrystallization of nuclear fuels ☆

J. Rest

Argonne National Laboratory, Energy Technology-212, 9700 S. Cass Avenue, Argonne, IL 60439-4815, USA

Received 1 October 2003; accepted 8 January 2004

Abstract

Irradiation-induced recrystallization appears to be a general phenomenon in that it is observed to occur in a variety of nuclear fuel types, e.g. U–*x*Mo, UO_2, and U_3O_8. For temperatures below that where significant thermal annealing of defects occurs, an expression is derived for the fission density at which irradiation-induced recrystallization is initiated that is athermal and weakly dependent on fission rate. The initiation of recrystallization is to be distinguished from the subsequent progression and eventual consumption of the original fuel grain. The formulation takes into account the observed microstructural evolution of the fuel, the role of precipitate pinning and fission gas bubbles, and the triggering event for recrystallization. The calculated dislocation density, fission gas bubble-size distribution, and fission density at which recrystallization first appears are compared to measured quantities.

1. Introduction

Irradiation-induced recrystallization of UO_2 nuclear fuels has been an active field of research since 1991 when the first theoretical description of this subject was published [1]. In addition, recrystallization has been observed to occur in other nuclear fuels, e.g. U–*x*Mo, where $6 \leqslant x \leqslant 10$, and U_3O_8 [2]. Three typical features characterize the process: Xe depletion, pore formation, and grain subdivision that appears sequentially as the local burnup increases [3]. In the pre-recrystallized regions of the material, high dislocation densities and small fission gas bubbles are observed [4,5]. The recrystallized regions show a predominant feature of ≈0.5–1 μm pores surrounded by sub-micron grains, with part of these grains being free of dislocations and gas bubbles [5–7]. The irradiation-induced recrystallization mechanism has been attributed to the diminution of potential recrystallization sites due to interaction (pinning) with vacancy–impurity pairs [1,8], the buildup of stored energy in the material due to irradiation damage [9], stresses produced as a result of over pressurized fission gas bubbles [10], instability phenomena [11], defect saturation [12], and atomic cascades induced by fission fragments [13]. However, none of the above models have satisfactorily explained all of the observed dependencies as well as the sequence of events leading up to recrystallization. For example, recrystallization is observed to initiate at pre-existing grain boundaries and/or the surfaces of large, pre-existing pores. In addition the onset of recrystallization in uranium–molybdenum alloy fuel for research reactor applications appears to be not at all, or very weakly, dependent on fuel temperature [2]. The evolution of the pre-recrystallized microstructure of the material is characterized by the transition from an interstitial-loop and tangled dislocation morphology [4] to that of a cellular (polygonized) dislocation network

☆ Work supported by US Department of Energy, Office of Arms Control and Nonproliferation, under Contract W-31-109-Eng-38.

E-mail address: jrest@anl.gov (J. Rest).

0022-3115/$ - see front matter © 2004 Elsevier B.V. All rights reserved.
doi:10.1016/j.jnucmat.2004.01.009

consisting of relatively low-angle sub-grains [14]. In addition, measurements of the change in the UO_2 lattice parameter in fuel that has a recrystallized rim structure show that the lattice parameter increases toward the pellet edge and decreases again within the recrystallized rim zone [15]. Models based on the evolution of the damaged microstructure indicate that the increase in lattice parameter can be attributed to the nucleation and growth of interstitial loops [16]. The subsequent decrease in lattice parameter within the recrystallized rim region occurs because of stress relaxation commensurate with the recrystallization process.

To date, models based on the evolution of the damage microstructure have not been satisfactorily interfaced with a triggering event for irradiation-induced recrystallization, and the role of gas bubbles in this process has not been clearly delineated. For example, several conflicting explanations have been put forward to account for evidence that xenon depletion, pore formation, and recrystallization begin at different local burnups [16]. In addition, a consensus has not been reached on the fission rate and temperature dependence of recrystallization [2,17], on the role of composition and fabrication parameters such as grain size [18], or on the role of stress [19]. This paper, presents a model for irradiation-induced recrystallization that links the observed microstructural evolution of the fuel, the role of fission gas bubbles, and the triggering event for recrystallization. In what follows, an expression is derived for the fission density at which irradiation-induced recrystallization is initiated. The initiation of recrystallization is to be distinguished from the subsequent progression and eventual consumption of original fuel grain. This latter process is not considered in this work.

2. Calculation of bubble-size distribution on potential recrystallization nuclei

The evolution of a cellular dislocation structure is assumed to be an integral step leading to irradiation-induced recrystallization. The walls of this cellular structure and/or the grain boundaries of the resulting sub-grain microstructure are considered to be potential recrystallization nuclei. Classical conditions for a viable recrystallization nucleus are a size advantage and a high interfacial mobility [20]. In an application of a rate-theory approach to the microstructural evolution of a cellular dislocation network, Rest and Hofman associated nanometer-size bubbles with the walls of the cellular dislocation structure [16]. These bubbles act as a dragging force on a moving boundary and thus reduce the interfacial mobility. If the bubbles are of sufficient size, the boundary will be effectively pinned and will be eliminated from the pool of potential recrystallization nuclei. To determine this effect, the gas bubble distribution on the boundaries of the cell wall and/or sub-grain structure needs to be assessed.

Let $n(r)\,\mathrm{d}r$ be the number of bubbles per unit volume on the cell walls (and/or sub-grain boundaries) with radii in the range r to $r+\mathrm{d}r$. Growth by gas atom collection from fission gas diffusing from the grain interior removes bubbles from this size range, but these are replaced by the simultaneous growth of smaller bubbles. The distribution of intragranular gas consists primarily of fission gas atoms due to the strong effect of irradiation-induced gas-atom re-solution. Bubbles appear on the cell walls and/or sub-grain boundaries due to the reduced effect of re-solution ascribed to the strong sink-like property of the boundary [21]. A differential growth rate between bubbles of different size leads to a net rate of increase in the concentration of bubbles in the size range r to $r+\mathrm{d}r$. This behavior is expressed by [22]

$$\left[\frac{\mathrm{d}n(r)}{\mathrm{d}t}\right]\mathrm{d}r = -\frac{\mathrm{d}}{\mathrm{d}r}\left[n(r)\frac{\mathrm{d}r}{\mathrm{d}t}\right]\mathrm{d}r. \tag{1}$$

The growth rate $(\mathrm{d}r/\mathrm{d}t)$ of a particular bubble is related to the rate $(\mathrm{d}m/\mathrm{d}t)$ at which it absorbs gas from the matrix. For the small cell and/or sub-grain sizes characteristic of the pre-recrystallized grain microstructure, the rate of precipitation is controlled by the gas-atom diffusion coefficient D and the average concentration C of fission gas retained in the lattice,

$$(\mathrm{d}m/\mathrm{d}t) = 4\pi DrC. \tag{2}$$

For the small bubbles that have been observed in the pre-recrystallized irradiated material [4], the relationship between size and gas content can be approximated by

$$m = (4\pi r^3/3b_\mathrm{v}), \tag{3}$$

where b_v is the van der Waals constant. Differentiating Eq. (3) and equating to Eq. (2) results in

$$\mathrm{d}r/\mathrm{d}t = b_\mathrm{v}DC/r. \tag{4}$$

The temperature range where irradiation-induced recrystallization is observed to occur is relatively low (below that where thermal annealing of defects occurs, e.g. in $UO_2 < 850$ °C). As such, the gas-atom diffusion coefficient D is expected to be athermal with negligible intergranular gas bubble mobility. Studies on the evolution of helium bubbles in aluminum during heavy-ion irradiation at room temperature have shown that bubble coarsening can take place by radiation-induced coalescence without bubble motion [23]. This coalescence is the result of the net displacement of Al atoms out of the volume between bubbles initially in close proximity. The resulting non equilibrium-shaped bubble evolves toward a more energetically favorable spherical shape whose final size is determined by the equilibrium bubble pressure.

Bubble coalescence without bubble motion can be understood on the basis of a difference in the probability for an atom to be knocked out of the volume between a pair of bubbles and the probability of an atom to be injected into this inter-bubble volume. If the bubbles contained the same atoms as that comprising the inter-bubble volume, the net flux of atoms out of the inter-bubble volume would be zero. However, since the gas bubbles contain fission gas and not matrix atoms, the flux of atoms into the inter-bubble volume is reduced by the bubble volume fraction, i.e., the net flux out of volume is equal to $\lambda V - \lambda(V - V_B)$, where λ is the atom knock-on distance, and V_B is the bubble volume fraction. It is assumed that most of the impacted atoms receive enough energy to travel distances λ on the order of the inter-bubble spacing. Thus, assuming that the atom displacement rate is proportional to the fission rate, the net rate of change in the concentration of bubbles in the size range r to $r + \mathrm{d}r$ due to bubble coarsening without bubble motion is given by

$$\left[\frac{\mathrm{d}n(r)}{\mathrm{d}t}\right]\mathrm{d}r = \frac{\mathrm{d}}{\mathrm{d}r}\left[\frac{2}{3}\lambda F\pi r^3 n(r)\right]\mathrm{d}r, \tag{5}$$

where F is the fission rate.

The overall net rate of change of the concentration of bubbles in a given size range is derived by subtracting the right-hand side of Eq. (5) from that of Eq. (1):

$$\frac{\mathrm{d}n(r)}{\mathrm{d}t}\mathrm{d}r = -\frac{\mathrm{d}}{\mathrm{d}r}\left[n(r)\frac{\mathrm{d}r}{\mathrm{d}t}\right]\mathrm{d}r - \frac{\mathrm{d}}{\mathrm{d}r}\left[\frac{2}{3}\lambda F\pi r^3 n(r)\right]\mathrm{d}r. \tag{6}$$

The equilibrium population of bubbles is obtained by setting Eq. (6) to zero

$$(b_v DC/r^2)n(r) - (b_v DC/r)\,\mathrm{d}n(r)/\mathrm{d}r - \frac{2}{3}\lambda F\pi r^3\frac{\mathrm{d}n(r)}{\mathrm{d}r} - 2\lambda F\pi r^2 n(r) = 0, \tag{7}$$

where Eq. (4) has been used for $\mathrm{d}r/\mathrm{d}t$.

Eq. (7) must be solved subject to the relevant boundary condition. The above calculation assesses the viability of potential recrystallization sites in terms of interfacial mobility in the presence of fission-gas bubbles attached to cell walls and/or sub-grain boundaries. Given this consideration, Eq. (7) is solved subject to the constraint that the constant of integration is determined by integrating Eq. (7) only over those bubbles that are located on potential nuclei. More bubbles than this may exist within the microstructure (e.g., on sub-grain surfaces), but the assumption here is that, at a minimum, one bubble inhabits every potential nucleus. Potential recrystallization nuclei are taken as the nodes, or triple points, of the cellular dislocation or sub-grain structure. If C_{rx}^0 is the initial density of such potential recrystallization nuclei, then the solution to Eq. (7) is

$$n(r) = \frac{4C_{rx}^0\sqrt{\kappa}r}{1+\kappa r^4}, \tag{8a}$$

where

$$\kappa = \frac{2\pi F\lambda}{3b_v DC}. \tag{8b}$$

3. Calculation of initial density of recrystallization nuclei

If, as discussed above, the potential recrystallization nuclei are taken to be the nodes, or triple points, of the cellular dislocation or sub-grain structure, then the density of these nodes is given by

$$C_{rx}^0 = 1/d_l^3, \tag{9}$$

where d_l is the cell size. An equation linking the cell size and the dislocation density, ρ_d, can be obtained by minimization of the total energy (dislocation line energy plus the energy stored in isolated terminating dislocation boundaries), as follows [24]:

$$d_l = C_A C_\rho\sqrt{\frac{\pi}{\rho_d f(v)}}, \tag{10}$$

where $f(v) = (1 - v/2)/(1 - v)$, v is Poisson's ratio, C_A is 3 for cubic cells, and C_ρ is within a factor of unity.

The steady-state mobile dislocation density can be determined as follows [25]. Consider a plane in the material upon which interstitial loops are nucleated at a rate K_{nl}. When equilibrium is achieved, the nucleation rate of new loops equals the annihilation rate K_{al}. If it is assumed that the loop annihilation rate is proportional to the number of loops, N_l, and inversely proportional to the distance between them, then

$$K_{al} = N_l^{3/2} v_0, \tag{11}$$

where v_0 is the rate of climb-controlled glide (i.e., it is assumed that loop glide across the plane to the cell walls is much faster than climb). The line length corresponding to the loops is

$$\rho_l = 4N_l D_l, \tag{12}$$

where the loop geometry is taken to be square, and D_l is the average loop size, taken to be equal to half the distance between them, i.e.,

$$D_l = \frac{1}{2N_l^{1/2}}. \tag{13}$$

If L is the distance between planes, then the density of planes is $3/(2L)$ and, from Eqs. ((11)–(13)), the dislocation density ρ_d is given by

$$\rho_d = \frac{3}{L}\left(\frac{K_{nl}}{v_0}\right)^{1/3}. \tag{14}$$

Under steady-state conditions $D_vC_v \approx D_iC_i$ (D_v, D_i and C_v, C_i are the vacancy and interstitial diffusivity and atom-fraction concentration, respectively), and the rate of dislocation climb is given by

$$v_0 = \frac{1}{b} B_i C_i D_i. \tag{15}$$

where b is the magnitude of the Burgers vector, and B_i is the relative bias between interstitials and vacancies for dislocations. The rate of interstitial loop nucleation can be expressed as

$$K_n = \alpha_i \frac{C_i^2 D_i}{2a^3}, \tag{16}$$

or, with reference to one plane,

$$K_{nl} = \alpha_i \frac{C_i^2 D_i L}{3a^3}, \tag{17}$$

where a is the lattice constant, and $\alpha_i = \sqrt{2}/a^2$ is the rate constant for nucleation of loops as di-interstitials. At temperatures less than one half of the melting temperature, defect loss due to recombination is dominant, and the interstitial concentration has an approximate solution given by

$$C_i = \frac{K}{D_i \alpha_r C_v}, \tag{18}$$

where K is the displacement rate, and $\alpha_r = 4\pi r_{iv}/\Omega$ is the rate constant for loss of defects due to recombination, r_{iv} is the radius of the recombination volume, and Ω is the atomic volume. Substituting the steady-state solution for the vacancy concentration in the limiting regime where recombination is dominant, i.e., $C_v = \sqrt{\frac{K}{D_v \alpha_r}}$ along with Eqs. (15)–(18) into Eq. (14) yields the following expression for the dislocation density:

$$\rho_d = \left(\frac{3}{La}\right)^{2/3} \left(\frac{\alpha_i}{B_i D_i}\right)^{1/3} \left(\frac{K D_v}{\alpha_r}\right)^{1/6}, \tag{19}$$

where the Burgers vector b has been taken equal to the lattice constant a. Finally, using Eq. (10) in Eq. (9) gives the following result for the initial density of recrystallization nuclei:

$$C_{rx}^0 = \frac{[\rho_d f(v)/\pi]^{3/2}}{(C_A C_\rho)^3}. \tag{20}$$

4. Calculation of the time-dependent density of recrystallization nuclei

Small fission gas bubbles are almost invariable associated with small precipitates [14,26,27]. Apparently, the small bubbles provide adequate space for the collection of impurity atoms. Based on these observations, it is assumed that fission gas bubbles containing precipitates are distributed on the walls of the cellular dislocation structure and/or the surfaces of the sub-grain boundaries according to Eq. (8). The assumption is also made that one bubble/precipitate exists at each potential nucleus (e.g. triple points of sub-grain boundary microstructure). Precipitates having a size greater than a critical value can pin the boundary and preclude subsequent boundary movement [28,29]. Thus, nodes that have a bubble/precipitate with size greater than a critical size r_{crit} will be pinned and will be eliminated from the pool of potential recrystallization nuclei. Here it has also been assumed that there is a correlation between bubble and precipitate size, i.e. the bubble size is greater or equal to then precipitate size. The density of viable recrystallization nuclei C_{rx} is obtained from Eq. (8) by integration over all bubble radii $r \geqslant r_{crit}$ and is thus given by the following expression:

$$C_{rx} = C_{rx}^0 \left[1 - \frac{4\sqrt{\kappa}}{\pi} \int_{rcrit}^{\infty} \frac{r\,dr}{(1+\kappa r^4)}\right]. \tag{21}$$

Upon evaluating the integral on the right-hand side of Eq. (21) the expression for C_{rx} can be simplified to

$$C_{rx} = \frac{2C_{rx}^0}{\pi} Tan^{-1}(\sqrt{\kappa} r_{crit}^2) \tag{22}$$

or

$$C_{rx} \approx \frac{2C_{rx}^0}{\pi} \sqrt{\kappa} r_{crit}^2 \tag{23}$$

for $\sqrt{\kappa} r_{crit}^2 \ll 1$.

5. Calculation of critical bubble/precipitate size

The sub-grain growth rate for randomly distributed precipitates is given by [30]

$$\frac{dR_s}{dt} = \frac{3}{2} \alpha M \tau \left(\frac{1}{R_s^0} - \frac{1}{R_s} - \frac{R_s f_p \gamma}{\alpha_p \pi r_p^2}\right), \tag{24}$$

where α_p is a constant of the order unity, M is the grain boundary mobility, f_p is the phase fraction of impurity particles of average radius r_p, R_s^0 is the average sub-grain size, and γ is a factor that takes into account the lower force which acts on the dislocations when the precipitates are passed by climb. Sub-grains that are smaller than a critical grain size will shrink and eventually disappear and the grains that are larger than the critical grain size will grow. The larger grains grow at the expense of the average sub-grains until the average sub-grains disappear. For a given phase fraction of precipitates f_p sub-grain growth will be precluded for precipitate sizes r_p greater than a critical precipitate size

r_{crit}. The condition for sub-grain growth is given by setting $dR_s/dt = 0$ in Eq. (24). In this manner an expression for r_{crit} can be derived and is given by

$$r_{crit} = \frac{3\alpha_p}{4n_p\gamma}\left(\frac{1}{2R_s^0}\right)^2, \tag{25}$$

where $n_p = f_p/(4\pi r_p^3/3)$ is the number of precipitates per unit volume, and the sub-grain radius at which accelerated growth is initiated is taken to be at $R = 2R_s^0$. Identifying the average sub-grain radius R_s^0 as $d_l/2$, where d_l is given by Eq. (10) and after substituting into Eq. (25) one obtains

$$r_{crit} = \frac{3\alpha_p f(v)\rho_d}{4n_p\gamma\pi(C_A C\rho)^2}. \tag{26}$$

If it is assumed that the majority of precipitate nuclei are formed by direct production then

$$n_p = \phi F_d, \tag{27}$$

where ϕ is the number of precipitate nuclei formed per fission event. Finally, substituting Eqs. (8b), (20), (26) and (27) into Eq. (23) the concentration of viable recrystallization nuclei becomes

$$C_{rx} = \frac{9(f(v)\rho_d)^{7/2}}{8\pi^6(C_A C_\rho)^7 F_d^{5/2}}\left(\frac{\alpha_p}{\phi\gamma}\right)^2\sqrt{\frac{2\lambda}{3\pi b_v B_0\beta}}, \tag{28}$$

where $F_d = Ft$ is the fission density, $C = \beta Ft$, and where, at the relatively low temperatures where irradiation-induced recrystallization occurs, the gas atom diffusivity is athermal and can be expressed as $D = B_0 F$, where B_0 is a constant of proportionality.

6. Calculation of trigger for irradiation-induced recrystallization

From a thermodynamic perspective, to become a viable recrystallization nucleus, a node must acquire a critical standard free energy ΔG^*. The equilibrium number of nuclei, n_i^* per unit volume is given by [31]

$$n_i^* = n_i^0 \exp(-\Delta G^*/kT). \tag{29}$$

The temperature dependence of C_{rx} in Eq. (28) is contained in the interstitial and vacancy diffusivities. In general, these diffusivities are expressed as $D_i = D_i^0\exp(-\varepsilon_i/kT)$ and $D_v = D_v^0\exp(-\varepsilon_v/kT)$, where ε_i and ε_v are the interstitial and vacancy migration enthalpies, respectively. Thus, comparing Eqs. (28) and (29) the critical standard free energy ΔG^* that a node must acquire in order to recrystallize is given by

$$\Delta G^* = \frac{7}{6}(\varepsilon_v/2 - \varepsilon_i) \tag{30}$$

and an expression for the critical fission density at which recrystallization will occur, F_{dx} can be derived as

$$F_{dx} = \frac{(f(v)\rho_d)^{7/5}\exp[7(\varepsilon_v/2-\varepsilon_i)/15kT]}{\pi^{12/5}(C_A C_\rho)^{14/5}(n_i^0)^{2/5}}\left(\frac{\alpha_p}{\phi\gamma}\right)^{4/5}\left(\frac{2\lambda}{3b_v B_0\beta}\right)^{1/5}, \tag{31}$$

where $F_{dx} = Ft_x$, where t_x is the time at which recrystallization is initiated.

It remains to determine n_i^0 in Eq. (31). It has been shown that the accumulation of dislocation loops leads to an increase in the lattice parameter [2] up to the point where recrystallization is initiated whereupon the lattice constant decreases [15]. n_i^0 is the basic entity out of which the clusters are composed. For example, in the theory of nucleation of liquid droplets in a vapor, n_i^0 is the number of single molecules per unit volume [31]. The basic unit out of which the cellular dislocation network is composed is the interstitial loop. n_i^0 is thus taken to be the athermal component in the expression for the loop density, i.e.,

$$n_i^0 = \left(\frac{\rho_l}{\pi d_l}\right)_{\text{Athermal}} = \frac{(C_A C_\rho)^2}{f(v)}\frac{(KD_v)^{1/4}}{\eta^3 D_i^{1/2}}\exp[+(\varepsilon_v/2 - \varepsilon_i)/2kT]. \tag{32}$$

Inserting the above expression into Eq. (31) results in the following expression for F_{dx}:

$$F_{dx} = \left[\frac{\alpha_p\rho_d}{\phi\gamma}\right]^{4/5}\left(\frac{\pi^2\lambda}{b_v B_0\beta}\right)^{1/5} \times \frac{f(v)^{6/5}\exp[4(\varepsilon_v/2 - \varepsilon_i)/15kT]}{\pi^{9/5}(C_A C_\rho)^{12/5}}. \tag{33}$$

For UO_2, substituting nominal values of the parameters $\{B_0 = 10^{-29}\ m^5,\ \varepsilon_v = 2.4\ eV,\ \varepsilon_i = 0.6\ eV\}$ [35], $\{\lambda = 220\ Å,\ F = 5\times10^{17}\ K\}$ [36], $\{v = 0.31,\ C_A = 3,\ C_\rho = 1\}$ [24], $L = 3\times10^{-8}$ m, and $\phi\gamma/\alpha_p = 2.3\times10^{-6}$ in Eq. (37) leads to the simplified expression for F_{dx} (m^{-3}):

$$F_{dx}(UO_2) = 8.3\times10^{29}/F^{2/15}. \tag{34}$$

The fission density at which recrystallization is predicted to initiate as given by Eq. (34) is athermal and very weakly dependent on fission rate.

7. Comparison of theory with data

In Fig. 1 the calculated dislocation density obtained using Eq. (19) is compared with data obtained at two different operating temperatures. In general, although the calculated results follow the trend of the data, the

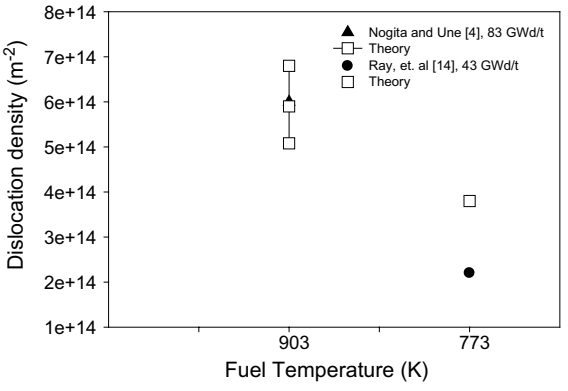

Fig. 1. Calculated dislocation density obtained using Eq. (19) compared with data as a function of temperature and burn.

calculation at the lower temperature is greater than the measured quantity. However, as reported in Ref. [4] '... when measuring the number of dislocations by the Ham method, it is very hard to separate extremely tangled dislocations.' The range of values for the calculated dislocation density for the 83 GWd/t fuel shown in Fig. 1 reflects the reported ±50 °C uncertainty in measured temperatures [5].

The total number of boundary bubbles per unit volume $N_{\rm gb}^{\rm V}$ can be estimated by solving Eq. (7) subject to the relevant boundary condition concerning the rate at which bubbles are formed at their nucleation size r_0. Nucleation is postulated to occur in regions of high defect concentration caused by the collision of fission fragments with the lattice. The highest defect concentrations are assumed to occur on or very near grain boundary surfaces and/or the surfaces of large pre-existing pores. Consequently, the rate of bubble nucleation is taken to be directly proportional to the rate of fission-product generation 2F. The constant of proportionality α ($\alpha = 0.25$ [22]) is the average number of bubbles induced to precipitate on the boundary by each fission fragment. It follows from a consideration of the growth rate of freshly nucleated bubbles that

$$n(r_0)\,{\rm d}r = (2F\alpha\,{\rm d}r)/({\rm d}r/{\rm d}t)_{r=r_0} \tag{35}$$

and by substitution from Eq. (4)

$$n(r_0) = 2F\alpha r_0/b_{\rm v}DC. \tag{36}$$

The solution of Eq. (7) subject to the boundary condition expressed by Eq. (36) is

$$n(r) = \frac{2F\alpha r}{b_{\rm v}DC}\,\frac{3b_{\rm v}DC + 2\pi F\lambda r_0^4}{3b_{\rm v}DC + 2\pi F\lambda r^4}. \tag{37}$$

Eq. (37) represents the total number of bubbles, i.e. those on potential nucleation sites and on the grain/cell surfaces. This is to be compared to Eq. (8) that represents the number of bubbles on the potential nucleation sites. The total concentration of bubbles on the boundaries is then given by

$$N_{\rm gb}^{\rm V} = \int_0^\infty n(r)\,{\rm d}r = \frac{\alpha F\pi(1+\kappa r_0^4)}{2\sqrt{\kappa}b_{\rm v}DC} = \frac{\alpha\pi(1+\kappa r_0^4)}{2\sqrt{\kappa}b_{\rm v}B_0\beta F_{\rm d}}. \tag{38}$$

Although it is true that, in general, the constant-density approximation given by Eq. (3) applies to bubbles on the order of 1 nm in size or smaller, for the relatively low temperatures under consideration in this paper ($T/T_{\rm M} < 0.4$) the contribution to Eq. (38) from bubbles having radii substantially larger than 10 nm is small.

The bubble density $N_{\rm gb}^{\rm V}$ as given by Eq. (38) is inversely proportional to the square root of the fission density. At $F_{\rm dx} = 1.8 \times 10^{27}$ fissions/m^3, $N_{\rm gb}^{\rm V} = 3 \times 10^{23}$ bubbles/m^3. The average value of the square of the bubble radius is given by

$$(r^2)_{\rm ave} = \frac{\int r^2 n(r)\,{\rm d}r}{\int n(r)\,{\rm d}r} = \frac{2}{\kappa^{1/2}}. \tag{39}$$

Thus, the average bubble radius is proportional to the fission density to the 1/4 power and has a value of 7.6 nm at $F_{\rm dx} = 1.8 \times 10^{27}$ fissions/m^3. This is to be compared to the value of $r_{\rm crit} = 4.5$ nm at this fission density.

Figs. 2 and 3 show the calculated bubble density (using Eq. (38)) and diameter (using Eq. (39)), respectively, as a function of burnup compared with data of Refs. [4,5]. In general, although the calculated quantities follow the trends of the data the calculated bubble density is somewhat lower and the bubble diameter somewhat higher than the measured quantities. The reason for this apparent discrepancy could be associated with the use of $C = \beta Ft$ for the average gas concentration in the lattice. This expression ignores the experimental observation that recrystallization appears to be

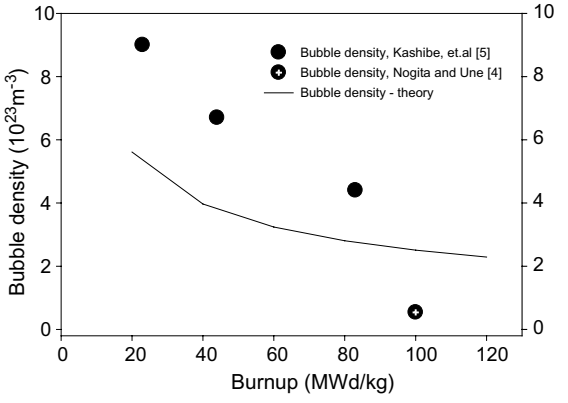

Fig. 2. Calculated bubble density as a function of fuel burnup obtained using Eq. (38) compared with data.

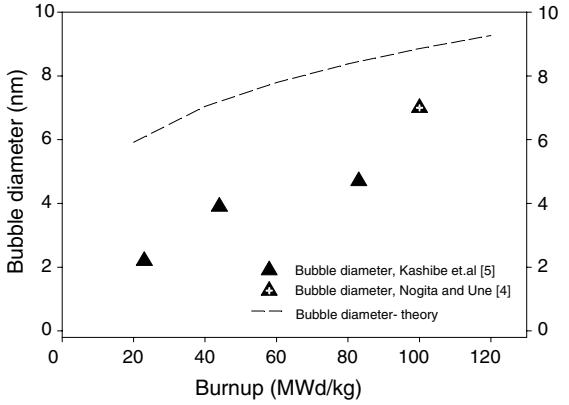

Fig. 3. Calculated bubble diameter as a function of fuel burnup obtained using Eq. (39) compared with data.

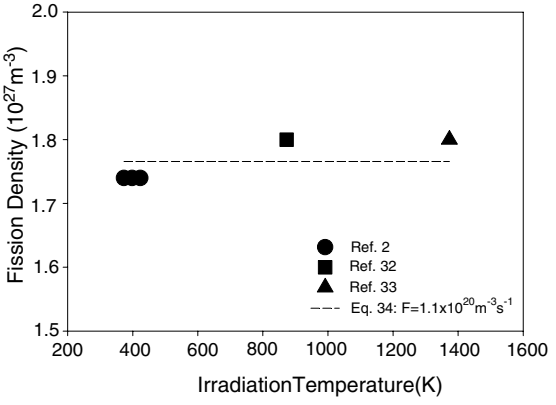

Fig. 5. Calculated recrystallization dose as a function of irradiation temperature obtained using Eq. (34) compared with data.

initiated on or near the original grain boundaries and/or the surface of large pre-existing pores. An assessment of the effect of original grain boundaries on recrystallization kinetics will be addressed in a future publication.

Fig. 4 shows the calculated bubble density as a function of bubble diameter obtained using Eqs. (38) and (39) compared with data. The theory relates the bubble density to the inverse square of the bubble diameter. This relationship reflects the assumed equilibrium nature of the gas bubbles. This result is to be compared to that of Ref. [5] where the bubble density was found to depend on the inverse of the bubble diameter to the 2.6 power. This dependence is characteristic of a mixed state comprised of equilibrium and over-pressurized bubbles.

Fig. 5 shows the fission density at which recrystallization is estimated to occur in uranium oxide fuels as a function of irradiation temperature. The average fission rate for the three irradiations shown in Fig. 5 were similar (i.e., $\approx 7.6\times10^{19}$–1.5×10^{20} m^{-3} s^{-1}). Also shown in Fig. 5 is the calculated dose using Eq. (34) with an average fission rate of 1.1×10^{20} m^{-3} s^{-1}. As is evident from Fig. 5 the theory follows the trends of the data [32,33].

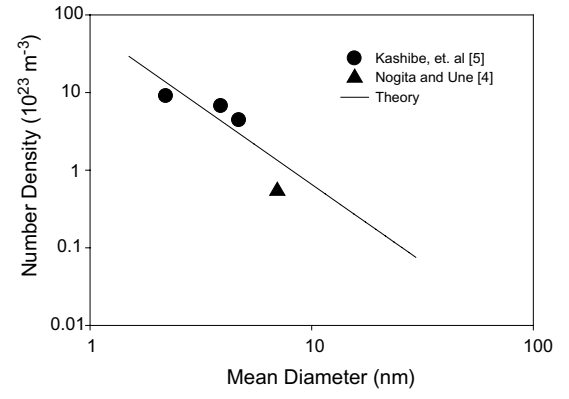

Fig. 4. Calculated bubble density as a function of bubble diameter obtained using Eqs. (38) and (39) compared with data.

8. Discussion

As shown by Eq. (33), the critical fission density at which recrystallization is predicted to occur is athermal (i.e., the temperature-dependent factors cancel each other out) and is inversely proportional to the atom-displacement (and, thus, fission) rate to the 2/15 power. The athermal temperature dependence of the critical fission density for uranium oxide fuels is demonstrated in Fig. 5. The theory presented in this paper is also consistent with recent observations of recrystallization in U–10Mo alloy fuel [1], where the onset of recrystallization occurs near the original grain boundaries and appears to be independent of temperature in the range of 350–550 K within a variation in fission rate of a factor of two. If one assumes that the temperature independence demonstrated in Fig. 5 for uranium oxide fuels applies to uranium metal alloys, then the observation reported in Ref. [1] supports the predicted weak fission-rate dependence given by Eq. (33). The similarity in recrystallization kinetics between uranium oxide and uranium alloy materials can be understood in terms of similarities in defect behavior. For example, in UO_2 describing dislocation behavior in terms of a single interstitial type (e.g. as in Eq. (15)) can be ascribed to the U^{4+} ion being the rate controlling species of the complex, whereas in U–10Mo the weighted average of uranium and molybdenum atoms is the rate-controlling species for diffusion.

If one assumes that the observed bubbles in the rim region are located at triple-point junctions, i.e., the sites

that comprise viable recrystallization nuclei, then the density of observed bubbles should be approximately equal to the density of these nodes. Spino et al. [6] derived a value of $\approx 10^{17}/m^3$ for the density of pores having an average diameter of 1.25 μm based on measured two-dimensional data at a fractional radial position of 0.996 in fuel that reached an average burnup of 40.3 GWd/t M. The density of viable recrystallization nuclei calculated from Eqs. (20) and (23) at $t = t_x$ (i.e., at the onset of recrystallization in UO_2) is $\approx 6 \times 10^{19}$ nuclei/m^3. At this point the initial density of nuclei (given by Eq. (20)) has been reduced a factor of 2.3. Given that some pore coalescence has most likely occurred between the onset of recrystallization where bubbles are in the nanometer size range and Spino's observation of micron size pores in the fully recrystallized rim region, this calculated value for the density of viable nuclei is consistent with the pore density estimated in Ref. [6].

The derivation of Eq. (33) is based on equivalence between the thermodynamic description given by Eq. (29) and a kinetic description given by Eq. (28). The concept of 'thermodynamic equilibrium' incorporates the requirement that there should be no fluxes passing through the system. Diffusion, however, is concerned with material transport and is a process which is essentially irreversible. In a state of equilibrium, diffusion fluxes should disappear. Nevertheless, a thermodynamic description, both as a means of approaching the phenomenon as well as a means for the calculation of parameters has been found to be extremely useful for the analysis of migration of atoms by diffusion [34]. Finally, reasonable agreement between theoretical predictions and experiment justifies assumptions upon which the theory is based, although, a priori, these assumptions might not appear to be well founded.

In the application of the previously developed irradiation-induced recrystallization model of Ref. [8] to irradiated UO_2 fuel at relatively low temperatures, an athermal diffusion coefficient is utilized for vacancy–impurity pairs that interact with and immobilize potential recrystallization nuclei. For vacancy migration enthalpies of ≈2 eV, the predicted fission density at which recrystallization occurs is proportional to 1/T and independent of fission rate. The relatively weak temperature dependence is due to the combination of athermal pair diffusion, recombination-dominated defect behavior, and recombination-dominated vacancy–impurity pair behavior that cancels out an exponential dependence on temperature. For migration enthalpies >2 eV both the fission rate and temperature dependence of the recrystallization dose become much stronger.

The new theory of irradiation-induced recrystallization described in this paper has several advantages over the model described in Ref. [8]. First, the present model provides for a mechanistic calculation of the evolution of the microstructure leading up to recrystallization whereas the previous model expressed the initial (equilibrium) density of recrystallization nuclei in terms of a formation enthalpy. Second, as shown in Fig. 5 for UO_2, and observations of the onset of recrystallization in U–10Mo fuel irradiated at different temperatures indicates that recrystallization in this material is athermal, or at a minimum, very weakly temperature dependent [2], consistent with the findings of the new theory. In addition, the new theory accounts naturally for observations of fission gas bubbles and precipitates in a defected microstructure [2,16].

The theory presented above relates the critical standard free energy ΔG^* that a node must acquire in order to recrystallize to the electronic properties of the material by $\Delta G^* = \frac{7}{6}(\varepsilon_v/2 - \varepsilon_i)$. The interstitial loop formation enthalpy (e.g., see Eq. (32)) is given by $(\varepsilon_v/2 - \varepsilon_i)/2kT$. Thus, the critical standard free energy ΔG^* that a node must acquire in order to recrystallize is 7/3 of the loop formation enthalpy. This relationship underlies the fundamental connection between damage microstructure and irradiation-induced recrystallization explored in this paper.

A consequence of Eq. (30) is that materials where $\varepsilon_i > \varepsilon_v/2$ have a negative ΔG^* and are precluded from recrystallization (and, equivalently, from interstitial loop formation). This may be the reason why bubbles have not been observed in certain irradiated materials. For example, bubbles resolvable with a scanning electr0on microscope (SEM) have not been observed in UAl_x [37]. Bubbles confined to the bulk (lattice) material cannot grow to appreciable sizes at low temperatures due to the effect of irradiation-induced re-solution. Only when sinks, such as grain boundaries, are present in the material can bubbles grow to SEM-observable sizes. The strong sink-like nature of a grain boundary provides a relatively short recapture distance for gas that has been knocked out of a bubble due to re-solution, and as such neutralizes the 'shrinking' effect of the re-solution process. These grain-boundary bubbles grow at an enhanced rate as compared to those in the bulk material [21].

Irradiation-induced recrystallization provides new grain boundaries upon which bubbles can nucleate and grow at an accelerated rate. Prior to recrystallization, SEM resolvable bubbles are generally not observed in UO_2 or in uranium alloy fuels. If recrystallization does not occur in UAl_x, then this would offer a basis for understanding the absence of such bubbles in SEM micrographs of the irradiated material at high burnup [37].

Substituting nominal values of the interstitial and vacancy migration enthalpies in UO_2 [35] ($\varepsilon_v = 2.4$ eV, and $\varepsilon_i = 0.6$ eV) into Eq. (34) gives $\Delta G^* \approx 0.7$ eV. The mobility of high angle grain boundaries is temperature dependent and is often found to obey an Arrhenius type relationship of the form

$$M = M_0 \exp\left(-\frac{Q}{RT}\right). \quad (40)$$

The apparent activation energy Q may be related to the atom-scale thermally activated process that controls boundary migration (and, thus, recrystallization). The value of Q for migration of high angle boundaries in metals of high purity is in the range of 0.25–1.25 eV [38]. This is to be compared to the value of $\Delta G^* \approx 0.7$ eV estimated above.

9. Conclusions

An expression is derived for the fission density at which various nuclear fuels undergo irradiation-induced recrystallization. It is based on the evolution of a cellular dislocation network upon which impurity atoms and fission gas bubbles nucleate and grow. The model assumes that most fission gas bubbles contain precipitates in accordance with experimental observation. The bubble-size distribution is calculated as a function of fission rate and temperature. Bubble coarsening occurs as a result of radiation-induced coalescence of bubbles without bubble motion. Precipitates that are greater than a critical size effectively pin triple-point nodes of the resulting sub-grain network, thus eliminating them as potential recrystallization nuclei. Recrystallization is induced when the density of viable recrystallization nuclei equals the equilibrium number of nuclei calculated based on thermodynamics. The basic entities out of which these nuclei are composed are interstitial loops. The resulting expression for the fission density at which recrystallization is predicted to initiate is athermal, and weakly dependent on fission rate. For UO_2, $F_{dx}(UO_2) = 8.3 \times 10^{29}/F^{2/15}$ m^{-3}. The critical standard free energy ΔG^* that a node must acquire in order to recrystallize is given by $\frac{7}{6}(\varepsilon_v/2 - \varepsilon_i)$. A consequence of this relationship is that materials that have $\varepsilon_i > \varepsilon_v/2$ are precluded from irradiation-induced recrystallization.

Acknowledgements

The author gives special thanks to Drs Jose Spino (ITU-Karlsruhe) and Gerard Hofman (ANL) for many interesting discussions.

References

[1] J. Rest, G.L. Hofman, in: S.E. Donnelly, J.H. Evans (Eds.), Fundamental Aspects of Inert Gases in Solids, Plenum, New York, 1991, p. 443.
[2] J. Rest, G.L. Hofman, in: Proceedings of Materials Research Society Meeting, Symposium R, Boston, MA, November 2000.
[3] J. Spino, D. Baron, M. Coquerelle, A.D. Stalios, J. Nucl. Mater. 256 (1998) 189.
[4] K. Nogita, K. Une, Nucl. Instrum. and Meth. B 91 (1994) 301.
[5] S. Kashibe, K. Une, K. Nogita, J. Nucl. Mater. 206 (1993) 22.
[6] J. Spino, K. Vennix, M. Coquerelle, J. Nucl. Mater. 231 (1996) 179.
[7] K. Nogita, K. Une, J. Nucl. Mater. 226 (1995) 302.
[8] J. Rest, G.L. Hofman, J. Nucl. Mater. 210 (1994) 187.
[9] L.E. Thomas, C.E. Beyer, L.A. Charlot, J. Nucl. Mater. 188 (1992) 80.
[10] Hj. Matzke, J. Nucl. Mater. 189 (1992) 141.
[11] M. Kinoshita, J. Nucl. Mater. 248 (1997) 185.
[12] D. Baron, B. Hermitte, J.P. Piron, in: Proceedings of IAEA Technical Committee Meeting on Advances in Pellet Technology for Improved Performance at High Burn-up, Tokyo, Japan, 1996, Paper 3/7.
[13] C.B. Lee, Y.H. Jung, J. Nucl. Mater. 279 (2000) 207.
[14] I.L.F. Ray, H. Thiele, Hj. Matzke, J. Nucl. Mater. 188 (1992) 90.
[15] J. Spino, D. Papaioannou, J. Nucl. Mater. 286 (2000) 146.
[16] J. Rest, G.L. Hofman, J. Nucl. Mater. 277 (2000) 231.
[17] M. Kinoshita, T. Kameyama, S. Kitajima, Hj. Matzke, J. Nucl. Mater. 252 (1998) 71.
[18] K. Nogita, K. Une, J. Nucl. Sci. Technol. 31 (9) (1994) 929.
[19] K. Une, K. Nogita, T. Shiratoni, K. Hayashi, J. Nucl. Mater. 288 (2001) 20.
[20] A.R. Jones, in: Grain Boundary Structure and Kinetics, American Society of Metals, Metals Park, 1980, p. 379.
[21] J. Rest, J. Nucl. Mater. 321 (2&3) (2003) 305.
[22] M.V. Speight, J. Nucl. Mater. 38 (1971) 236.
[23] R.C. Birtcher, S.E. Donnelly, C. Templier, Phys. Rev. B 50 (1994) 764.
[24] N. Hansen, D. Kuhlmann-Wilsdorf, Mater. Sci. Eng. 81 (1986) 141.
[25] I. Konovalov, Bochvar Institute, Moscow, Russia, Personal communication, 1999.
[26] I.L.F. Ray, H. Thiele, Hj. Matzke, in: S.E. Donnelly, J.H. Evans (Eds.), Fundamental Aspects of Inert Gases in Solids, Plenum, New York, 1991, p. 457.
[27] I.L.F. Ray, H. Thiele, Hj. Matzke, J. Nucl. Mater. 188 (1992) 90.
[28] S.J. Zinkle, R.A. Dodd, G.L. Kulcinski, in: F.A. Garner, J.S. Perkin (Eds.), Proceedings of Effects of Radiation on Materials 12th International Symposium, American Society for Testing and Materials-STP, 870, American Society for Testing and Materials, Philadelphia, 1985, p. 363.
[29] T. Sonoda, M. Kinoshita, I.L.F. Ray, T. Wiss, H. Thiele, D. Pellottiero, V.V. Rondinella, Hj. Matzke, Nucl. Instrum. and Meth. B 191 (2002) 622.
[30] R. Sandstrom, Acta Met. 25 (1977) 905.
[31] D. Turnbull, in: F. Seitz, D. Turnbull (Eds.), Phase Changes in Solid State Physics, vol. 3, Academic Press, New York, 1956, p. 225.
[32] J.D.B. Lambert, in: Metallurgical Society Conference on High Temperature Nuclear Fuels, vol. 42, Gordon and Breach, New York, 1968, p. 237.

[33] M.L. Bleiberg, r.M. Berman, B. Lustman, in: Proceedings of Symposium on Radiation Damage in Solid and Reactor Materials, IAEA, Vienna, 1963, p. 319.
[34] B.S. Bokshtein, S.Z. Bokshtein, A.A. Zhukhovitskii, Thermodynamics and Kinetics of Diffusion in Solids, Metallurgiya, Moscow, 1985, p. 9.
[35] Hj. Matzke, Radiat. Eff. 53 (1980) 219.
[36] D.R. Olander, Fundamental Aspects of Nuclear Reactor Fuel Elements, Technical Information Center, ERDA, USA, 1976, p. 291.
[37] G.L. Hofman, Nucl. Technol. 77 (1987) 110.
[38] F.J. Humphreys, M. Hatherly, Recrystallization and Related Annealing Phenomena, Pergamon, Oxford, 1995, p. 96.